Algorithm Technical Background Document

MODIS FIRE PRODUCTS

(Version 2.3, 1 October 2006)

(EOS ID# 2741)

Christopher Justice, Louis Giglio, Luigi Boschetti, David Roy, Ivan Csiszar, Jeffrey Morisette, and Yoram Kaufman

(MODIS Science Team)

ABSTRACT

The fire product is an interdisciplinary product designed to meet the needs of the global change research and the fire applications community. The product was developed in response to a growing demand for spatially explicit fire data to parameterize and validate various regional and global models. Fire is an important component of trace gas and particulate emission modelling, climate modelling, atmospheric transport and chemistry models, ecosystem dynamic models and models of land use change. Fire is also a land management issue and a natural hazard.

The MODIS fire products use the 1 km fire channels at 3.9 and 11 μm. Fire observations are made four times a day from the Terra AM (10:30 and 22:30) Aqua and PM (13:30 and 01:30) platofrms. As there is no on-board calibration for the high-temperature detectors, the pre-launch calibration of the high gain channels will be augmented with post-launch vicarious calibration. The MODIS products build on heritage algorithms for operational fire monitoring used with the GOES and AVHRR sensors, and provide information on the location of a fire, its emitted energy, the flaming and smoldering ratio, and an estimate of area burned.

In Memoriam

In the early years of MODIS, the approach to the active fire algorithm was developed in close cooperation with Dr. Yoram Kaufman and his team at NASA GSFC. We had many useful discussions on the physics of fire and the design and utility of the product, which shaped much of what has been done. Yoram was instrumental in the early development of the MODIS fire product and fire characterization and its application to aerosol studies. His continuing contribution to the evolution of the product is sorely missed.

Table of Contents

1. INTRODUCTION

The MODIS fire products build and improve on the experience of fire assessment primarily using the NOAA-AVHRR and GOES systems. Currently no other system provides the instrument characteristics needed for an effective global fire monitoring program. The MODIS sensor was designed to include characteristics specifically for fire detection and provides a unique capability over existing sensors in terms of fire monitoring. The fire products include an identification of the occurrence of thermal anomalies, an estimate the total emitted power from the fire and burned area.

Many users are ultimately interested in the area of land that is burned. This can be obtained through detection of burn scars. MODIS offers unique spatial and radiometric capabilities for burn scar detection. An automatic procedure for burn scar detection has been developed has now been implemented in the MODIS production stream. The products are available at full resolution and as spatial summaries and temporal composites.

The products are in differing stages of maturity and each product has an explicit validation program.

2. OVERVIEW AND TECHNICAL BACKGROUND

2.1 SCIENCE RATIONALE

The MODIS fire products provide an important input to research programs in several in different scientific disciplines. Fire is an important process within a most terrestrial biomes, and the release of gases and particulate matter during biomass burning is an important contributor to the chemical reactions and physical processes taking place in the atmosphere. Fire is a significant and continuous factor in the ecology of savannas, boreal forests and tundra, and plays a central role in deforestation in tropical and sub-tropical regions. In addition, on a periodic basis, extensive fire occurs in many temperate biomes such as forests, grasslands, and chaparral.

Monitoring the location and areal extent of biomass burning and its associated effects are important in the context of the goals and objectives of the US Global Change Research Program:

- Fire changes the physical state of the vegetation, releasing a variety of greenhouse gases into the atmosphere. There is presently great uncertainty as to the magnitude of the sources and sinks of these greenhouse gases. For example, the net annual release of carbon into the atmosphere due to the clearing and conversion of tropical forests for agricultural purposes (where biomass burning is a key tool used in the conversion process) is thought to contribute approximately 30% to the net annual increase in the concentration of atmospheric CO_2. In addition, there is an interest in changes in regional fire regimes under different climate change scenarios. For example, arguments have been made that an increase in average air temperature in northern latitudes will lead to a decrease in the natural fire return interval and an increase in fire severity in boreal forest and tundra ecosystems. This in turn, could lead to a significant reduction of the carbon stored in these ecosystems, with a comparable increase in atmospheric carbon.
- The release of chemically-reactive gases during biomass burning strongly influences chemical processes within the troposphere. In tropical regions, biomass burning has been shown to strongly influence regional and global distributions of tropospheric ozone and

has been related to acid deposition. Studies have shown that intensive biomass burning associated with naturally occurring forest fires, deforestation practices and savanna management is a major source of trace gases such as NO, CO_2, CO, O_3, NO_x, N_2O, NH_3, SO_x, CH_4, other non-methane hydrocarbons, as well as an abundant source of aerosols (Stith et al., 1981; Crutzen et al., 1985; Fishman et al., 1986; Andreae et al., 1988; Browell et al., 1988; Kaufman et al., 1992). Preliminary global estimates indicate that annual biomass burning may be associated with 38% of the ozone in the troposphere; 32% of global carbon monoxide; more than 20% of the world's hydrogen, nonmethane hydrocarbons, methyl chloride and oxides of nitrogen; and approximately 39% of the particulate organic carbon (Levine, 1991; Andreae, 1991). Although these estimates include a wide range of uncertainty, it is becoming evident that these emissions may be as important to global atmospheric chemistry as industrial activities in the developed world (Crutzen et al., 1985; Crutzen and Andreae, 1990). It is estimated that as much as 70 to 80% of the total biomass burned globally each year is burned in the equatorial and subtropical regions (Greenburg et al., 1984; Andreae, 1991). Some of the most intensive biomass burning activities are associated with deforestation and grassland management in South America, South East Asia and sub-Saharan Africa (Malingreau, 1990). The tropics receive the maximum amount of visible and ultra-violet radiation, thus acting as a primary driving force for atmospheric circulation. Since most biomass burning in the tropics is limited to a burning season, the temporal and spatial concentration of emissions are expected to have a noticeable impact on atmospheric chemistry and climate in the tropics and globally as a result of increased trace gas emissions and the direct and indirect radiative effects of smoke aerosols.

- The release of soot and other particulate matter during fires leads to significant physical changes within the troposphere in the region down-wind from the fire effecting air quality. First, depending on the single scattering albedo, particulate matter can result in a warming or cooling of the climate. Second, particles emitted from fires can effect cloud microphysics and radiative properties. The particles serve as cloud condensation nuclei and result in an increase in cloud cover and more reflective clouds. This increase in cloud cover increases the albedo of the atmosphere and reduces the average air temperature. In addition, these clouds also affect precipitation patterns. Recent analyses have indicated that the direct and indirect radiative effects of aerosols from biomass burning may be significant to the radiative balance of the earth and may be a major factor in climate change (Coakley et al., 1983; Twomey et al., 1984; Charlson et al., 1991; Kaufman et al., 1991; Twomey, 1991; Penner et al., 1992). Although the overall effects of aerosol loading from biomass burning are not very well understood. The two primary radiatively active components of aerosol emissions from biomass burning are particulate organic and graphitic carbon. Particulate organic carbon is the largest constituent and generally serves to scatter incoming solar radiation, while graphitic carbon particles can increase the solar radiation absorption in the atmosphere and clouds. The primary direct effect of particulate organic carbon aerosols is that they reflect incoming solar radiation back to space and act to cool the surface. The indirect effects of particulate organic carbon are associated with the ability for these aerosols to act as cloud condensation nuclei (CCN). Clouds are one of the most important controls on the heat balance of the earth.

A number of studies have been done to characterize the effects of aerosols due to anthropogenic pollution and biomass burning on clouds and climate (Stith et al., 1981; Twomey et al., 1984; Coakley et al., 1987; Hallett et al, 1989; Hudson, 1991; Rogers et al., 1991; Leaitch, et al., 1992). For thin to moderate clouds, increased CCN loading is thought to result in an increase in reflectivity and cloud albedo. Increased CCN loading generally results in increased droplet formation of a smaller size given a constant amount of available water. Clouds which are made of smaller droplets are usually assumed to be whiter, reflect more solar radiation and may be less likely to produce rain (Radke et al., 1990; Andreae, 1991). Previous results obtained by Kaufman and Nakajima (1993), which focused mainly on low level cumulus and stratocumulus clouds, indicated that in the Amazon high concentrations of smoke aerosols lead to a decrease in the cloud drop size but actually reduced the reflectivity of related clouds as a result of absorption by graphitic carbon. These results are consistent with those presented by Twomey (1977), which suggested that for optically thin clouds an increase in cloud drop concentration would result in a greater reflectivity, while for clouds which are optically thick and very bright to begin with, the effect of increased cloud drops would be dominated by absorption and reduction of cloud brightness.

- The results of natural fire or processes associated with fire affect the exchange of energy and water between land surfaces and the atmosphere. Fires can result in a decrease in the surface albedo and increase in the amount of solar radiation reaching the soil layer at local and regional scales. These, in turn, increase the amount of absorbed energy from incoming solar radiation, and generally increase the ground temperature. The changes in ground temperature affect a wide range of processes, including nutrient and water availability and microbial respiration. Removal of the plant canopy during fire reduces the amount of evapotranspiration and typically results in more water runoff. In tropical forests, the land clearing associated with biomass burning has resulted in a significant reduction of total precipitation in the region, and increase the surface runoff, soil erosion and river sedimentation. In tropical forests, activities associated with biomass burning and land clearing lead to an overall reduction in the amounts of precipitation in regions down-wind from the affected areas. First, the smoke from fires act as cloud condensation nuclei, and form additional water droplets in clouds; however, these droplets are typically smaller than those found in clouds found over tropical regions, and result in lower levels of precipitation. Second, land clearing and continuous burning leads to the conversion of forest to savanna. The grasses dominating the savannas have a much lower rate of evapotranspiration than trees, resulting in less water being returned to the atmosphere. Finally, savannas are much more susceptible to surface runoff, resulting in more precipitation flowing into streams and rivers. In addition, once the overlying vegetation of a tropical forest has been removed the exposed soil surface then becomes susceptible to erosion and the wetland and river systems are subject to sedimentation.

  In boreal forests, there is a dependence on the melting and formation of permafrost and the occurrence of fire, which in turn has a strong influence on the hydrology of these sites. In boreal forests, fire effects the flow of energy between the atmosphere and ground layer dramatically. First, fire removes a large portion of the vegetation layer which shades the ground, thus increasing the solar energy reaching the ground. Second, it decreases the albedo of the ground layer, increasing the amount of

energy absorbed by the ground layer. And third, fire removes much of the dead organic matter layer which insulates the ground. It has been shown that during the first year after a fire in a black spruce forest underlain by permafrost, there is a 5K to 7K increase in the temperature of the ground layer, which in turn causes a melting of the permafrost layer and an increase in the soil moisture in the active layer. The ground layer of these fire-affected areas remains affected for at least 15 to 25 years, with the depth of thaw of the active layer increasing also. Because of the melting permafrost and lack of a transpiring vegetation layer, during the initial years after a fire there is an increase in the moisture of the ground layer; however, after a few years, when the active layer becomes deeper, there is better drainage for the surface moisture, which then decreases. Finally, after about 20 to 25 years, the ground layer becomes cooler (as the vegetation layer becomes re-established, along with an increase in the depth of the dead organic matter layer), the active layer becomes shallower, and the ground layer moisture increases because of poorer drainage.

- Fires have several direct and indirect effects on terrestrial ecosystems. First, the pattern of fire (which includes its spatial distribution, fire return interval, and severity of burning) directly controls plant community development within those landscapes where biomass burning occurs. Fire favors those plants and tree species which have developed adaptations to fire (e.g., vegetative reproduction and fire-resistant seeds and cones) and eliminates those species which are less resistant to fire. Second, fire indirectly affects plant community development in a variety of ways, including (a) addition of key plant nutrients through ash fertilization or increased soil decomposition; (b) depletion of key plant nutrients through surface runoff or increased soil leaching; and (c) altering soil temperature and moisture. Finally, chemical reactions of the gases released by fire leads to an increase in atmospheric ozone and the deposition of acidic compounds downwind from fires, which in turn can effect the physiology of plants and ecosystems in these areas.

Fire has been identified by the international community as being an important variable for the Global Climate Observing System and an essential climate variable for the Franework Convention on Climate Change.

3. MODIS ACTIVE-FIRE ALGORITHM DESCRIPTION

3.1 THEORETICAL DESCRIPTION

The MODIS fire detection and characterisation techniques are fully automated for the production of daily, global fire information. In order to detect the presence of fire in a non-interactive fashion, a set of detection criteria different for the day and night fire observations are prescribed. These multipsectral criteria are based on the apparent temperature of the fire pixel and the difference between the fire pixel and its background temperature.

3.1.1 PHYSICS OF THE PROBLEM

The distinct flaming and smoldering fire stages are characterized by different fire intensity, temperature, and emission ratios. In several field experiments in Brazil Ward et al., measured 2-3 times as much emission of aerosol particles, CH_4 and NMHC in the smoldering phase as in the flaming phase (Ward et al., 1992; Kaufman et al., 1992). Therefore it is important to be able to distinguish between these two phases. The availability of oxygen to the fire, is a function of the fire intensity and structure. It determines the fraction of burned carbon released as CO and the fraction of black carbon in the aerosol particles (Crutzen and Andreae, 1990). The fire intensity and structure affect the fire temperature and the spatial extent of the hot zone.

Smoldering and flaming can be distinguished using infrared remotely-sensed measurements only if the fire temperatures vary significantly between these two stages. Based on a review of fire properties by Lobrt and Warnatz (1993) flaming temperature can be anywhere between 800 K and 1200 K, and as hot as 1800 K. Smoldering should be under 850 K and above 450 K. The actual range is probably smaller. The algorithm and sensitivity studies were based, therefore, on the assumption that the flaming temperature is 1000 K ± 200 K and the smoldering temperature is 600 K ± 100 K.

In a given fire pixel we may have areas that are not burned, areas that are smoldering and areas that are in flames. Figure 1 demonstrates the sensitivity of various MODIS channels to the fraction of the pixel covered by flames of 1000K (f_{flame}), and fraction of the pixel covered by smoldering of 600K (f_{smold}). The rest of the pixel is in temperature of 300K. The shorter the wavelength, the stronger the sensitivity to the higher temperature region. The main results are summarized in Table 1.

The 1.65 μm channel is very sensitive to f_{flame} and the flaming energy and not very sensitive to f_{smold} and its energy. The 2.13 μm channel is very sensitive to f_{flame} and somewhat sensitive to f_{smold}. Since the thermal energy is more concentrated in the flaming fire, the sensitivity to thermal energy is independent of smoldering or flaming. Unfortunately the MODIS 2.13 μm channel saturates at a reflectance of 0.8, which for the low solar brightness corresponds to less than 1% of the 500 m pixel being in flames. The importance of this channel is therefore limited. The 4 μm channel is sensitive to both f_{flame} and f_{smold}, and is five times more sensitive to the thermal energy emitted from flaming than from smoldering. Fig. 2 shows the effect of fire size and temperature on the apparent temperature of the pixel at 4 μm. This channel is sensitive to fires as small as 10^{-4} of the fire pixel.

The 4 µm channel response in daytime may be strongly enhanced by surface reflection where the satellite-surface-solar geometry results in sunglint. This effect has been documented over oceans (Nath et al., 1993; Cracknell, 1993) and can lead to false fire detections over land (Alberto Setzer, pers. comm.). Therefore the MODIS fire algorithm tests for sun glint and excludes those pixels from the fire products.

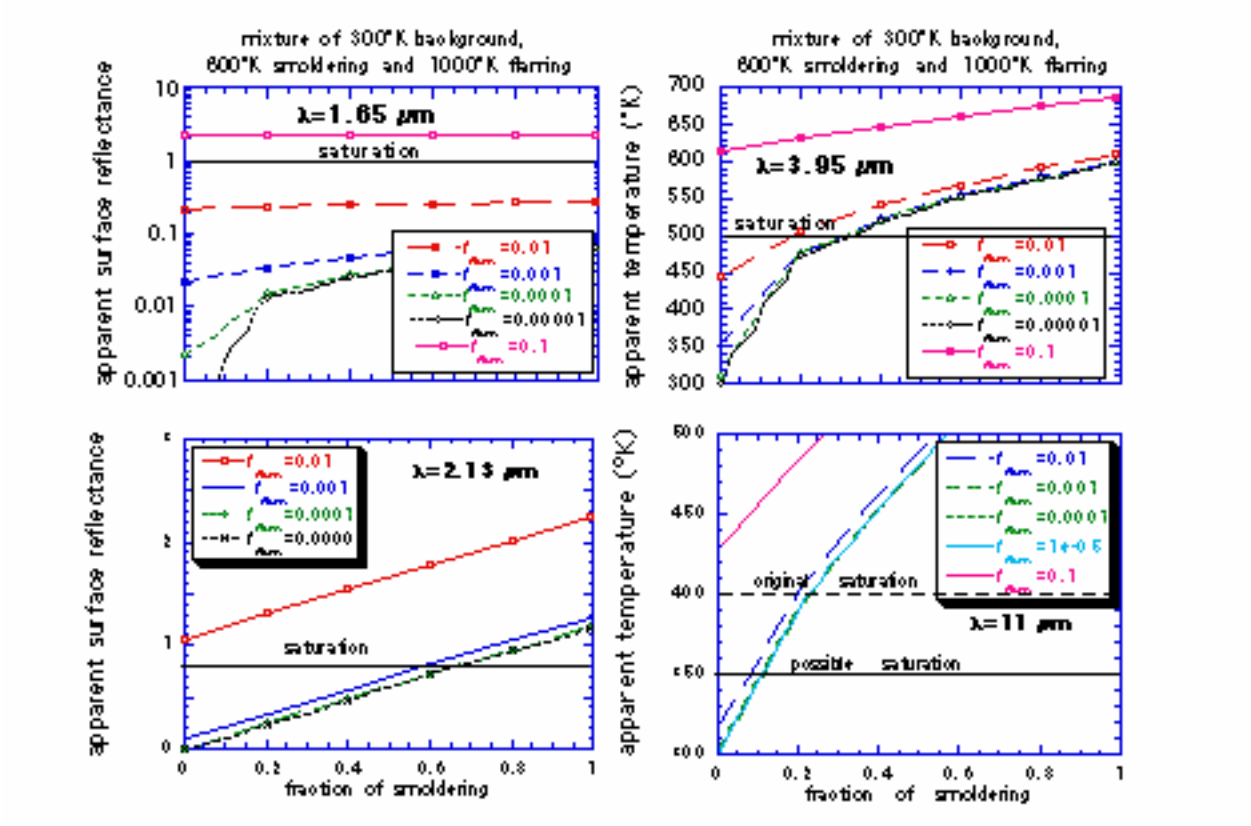

Fig. 1: The sensitivity of the MODIS channels to the fraction of the pixel covered by flames of 1000K (f_{flame}), and fraction of the pixel covered by smoldering of 600 K. The rest of the pixel is assumed to have a temperature of 300 K.

*Table 1: Information on the MODIS bands that can be used for fire detection. The saturation is given in reflectance units for the solar bands (ρ)or in temperature units (T) for the thermal bands. The sensitivity is given in kelvins change (Δ*T*) per change in the area covered by fire (*f*) or in change in the apparent surface reflectance (Δρ).*

channel	**spatial resolution**	**saturation**	**fraction of pixel that saturates the channel**		**sensitivity (Δρ/Δ*f*) and (Δ*T*/Δ*f*) at 600 K**	**sensitivity (Δρ/Δ*f*) and (Δ*T*/Δ*f*) at 1000 K**
			at 1000K	**at 600K**		
1.65 μm	500 m	ρ = 1 (740 K)	0.05	no saturation	Δρ/Δ*f* = 0.064	Δρ/Δ*f* = 220
2.13 μm	500 m	ρ = 0.8 (570 K)	0.007	0.65	Δρ/Δ*f* = 1.2	Δρ/Δ*f* = 110
3.96 μm	1000 m	500 K	0.025	0.30	Δ*T*/Δ*f* = 800 at *f* = 0.05	Δ*T*/Δ*f* = 8300 at *f* = 0.005
11 μm	1000 m	400 K	0.07	0.25	Δ*T*/Δ*f* = 485 at *f* = 0.05	Δ*T*/Δ*f* = 1700 at *f* = 0.005

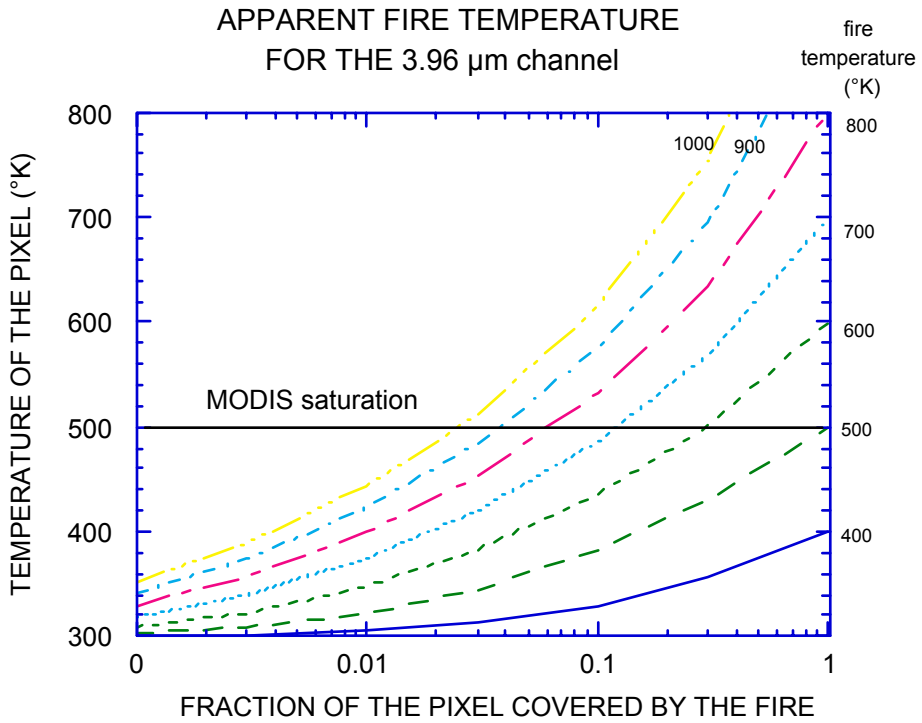

Fig. 2: The apparent temperature of the pixel at 3.96 μm, as observed by MODIS, for a single fire as a function of the fraction of the pixel covered by the fire and its temperature.

3.1.2 FIRE DETECTION

Fire detection is performed using a contextual algorithm (Giglio et al., 2003) that exploits the strong emission of mid-infrared radiation from fires (Dozier, 1981; Matson and Dozier, 1981). The algorithm examines each pixel of the MODIS swath, and ultimately assigns to each one of the following classes: *missing data*, *cloud*, *water*, *non-fire*, *fire*, or *unknown*.

The algorithm uses brightness temperatures derived from the MODIS 4 μm and 11 μm channels, denoted by T_4 and T_{11}, respectively. The MODIS instrument has two 4 μm channels, numbered 21 and 22, both of which are used by the detection algorithm. Channel 21 saturates at nearly 500 K; channel 22 saturates at 331 K. Since the low-saturation channel (22) is less noisy and has a smaller quantization error, T_4 is derived from this channel whenever possible. However, when channel 22 saturates or has missing data, it is replaced with the high saturation channel to derive T_4. T_{11} is computed from the 11 μm channel (channel 31), which saturates at approximately 400 K. The 12 μm channel (channel 32) is used for cloud masking; brightness temperatures for this channel are denoted by T_{12}.

The 250~m resolution red and near-infrared channels, aggregated to 1 km, are used to reject false alarms and mask clouds. The 500-m 2.1 μm band, also aggregated to 1 km, is used to reject water-induced false alarms. A summary of all MODIS bands used in the algorithm is shown in Table 2.

Pixels lacking valid data are immediately classified as *missing data* and excluded from further consideration. Cloud and water pixels are identified using an internal cloud mask and the water mask a within the MODIS Level 1A geolocation products (MOD13 and MYD03), and are respectively assigned the classes *cloud* and *water*. Processing continues on the remaining clear land pixels.

A preliminary classification is used to eliminate obvious non-fire pixels. For those potential fire pixels that remain, an attempt is made to use the neighboring pixels to estimate the radiometric signal of the potential fire pixel in the absence of fire. Valid neighboring pixels in a window centered on the potential fire pixel are identified and are used to estimate a background value. The window starts as a 3×3 pixel square ring around the potential fire pixel. Due to the triangular along-scan response of the MODIS instrument (Kaufman et al., 1998b), the two along-scan pixels adjacent to the potential fire pixel are deemed unreliable and excluded from the background characterization. The ring is increased to a maximum of 21×21 pixels, as necessary, until at least 25% of the pixels within the window have been deemed valid, and the number of valid pixels is at least eight. During this step, an optimized nearest-neighbor search is used to correct for the ``bowtie'' effect, or overlap between MODIS scans (Nishihama et al., 1997).

If the background characterization was successful, a series of contextual threshold tests are used to perform a relative fire detection. These look for the characteristic signature of an active fire in which both 4 μm brightness temperature and the 4 and 11 μm brightness temperature difference depart substantially from that of the non-fire background. Relative thresholds are adjusted based on the natural variability of the background. Additional specialized tests are used to eliminate false detections caused by sun glint, desert boundaries, and errors in the water mask. Candidate fire pixels that are not rejected in the course of applying these tests are assigned a class of *fire*. Pixels for which the background characterization could not be performed, i.e. those having an insufficient number of valid pixels, are assigned a class of *unknown*.

See *Giglio et al.* (2003) for a detailed description of the detection algorithm.

Table 2: MODIS channels used for active-fire detection and characterization.

Channel	Central wavelength (μm)	Purpose
1	0.65	Sun glint and coastal false alarm rejection; cloud masking.
2	0.86	Bright surface, sun glint, and coastal false alarm rejection; cloud masking.
7	2.1	Sun glint and coastal false alarm rejection.
21	3.96	High-range channel for fire detection and characterization.
22	3.96	Low-range channel for fire detection and characterization.
31	11.0	Fire detection, cloud masking.
32	12.0	Cloud masking.

3.1.3 FIRE CHARACTERIZATION

For each fire pixel detected, the *fire radiative power* (FRP) within the pixel is estimated using the empirical relationship of Kaufman et al. (1998):

$$\mathrm{FRP} = (4.34 \times 10^{-19}\,\mathrm{MW\,K^{-8}\,km^{-2}})(T_4^8 - \overline{T}_4)A_{\mathrm{pix}},$$

where T_4 is the 4-μm brightness temperature of the fire pixel, $\overline{T}_4$ is the mean 4-μm brightness temperature of the non-fire background, and A_{pix} is the total area (in km^2) of the pixel in which the fire was detected. The resulting value of the FRP is expressed in MW.

3.2 THE MODIS ACTIVE FIRE PRODUCTS

Descriptions of the current standard MODIS fire products are provided in the following five sections. More detailed descriptions can be found in the MODIS Active-Fire Product User's Guide[1].

3.2.1 LEVEL 2 FIRE PRODUCTS: MOD14 (TERRA) AND MYD14 (AQUA)

This is the most basic fire product in which active fires and other thermal anomalies, such as volcanoes, are identified. The Level 2 product is defined in the MODIS orbit geometry covering an area of approximately 2340 by 2030 km in the across- and along-track directions, respectively. It is used to generate all of the higher-level fire products, and contains the following components:

- An active fire mask that flags fires and other relevant pixels (e.g. cloud);
- a pixel-level quality assurance (QA) image that includes 19 bits of QA information about each pixel;
- a fire pixel table which provides 19 separate pieces of radiometric and internal-algorithm information about each fire pixel detected within a granule;
- extensive mandatory and product-specific metadata;

[1] http://modis-fire.umd.edu/products.asp

- a grid-related data layer to simplify production of the Climate Modeling Grid (CMG) fire product (see Section 3.2.5).

Product specific metadata within the Level 2 fire product includes the number of cloud, water, non-fire, fire, unknown, and other pixels occurring within a granule to simplify identification of granules containing fire activity.

3.2.2 LEVEL 2G DAYTIME AND NIGHTTIME FIRE PRODUCTS: MOD14GD/MOD14GN (TERRA) AND MYD14GD/MYD14GN (AQUA)

The Level 2 active fire products sensed over daytime and nighttime periods are binned without resampling into an intermediate data format referred to as Level 2G. The Level 2G format provides a convenient geocoded data structure for storing granules and enables the flexibility for subsequent temporal compositing and reprojection. The Level 2G fire products are a temporary, intermediate data source used solely for producing the Level 3 fire products and are consequently not available from the permanent MODIS data archive.

3.2.3 LEVEL 3 8-DAY DAILY COMPOSITE FIRE PRODUCTS: MOD14A1 (TERRA) AND MYD14A1 (AQUA)

The MODIS daily Level 3 fire product is tile based, with each product file spanning one of the 460 MODIS tiles, 326 of which contain land pixels (Figure 3). The product is a 1-km gridded composite of fire pixels detected in each grid cell over each daily (24-hour) compositing period. For convenience, eight days of data are packaged into a single file.

3.2.4 LEVEL 3 8-DAY SUMMARY FIRE PRODUCTS: MOD14A2 (TERRA) AND MYD14A2 (AQUA)

The MODIS daily Level 3 8-day summary fire product is tile-based, with each product file spanning one of the 460 MODIS tiles, of which 326 contain land pixels. The product is a 1-km gridded composite of fire pixels detected in each grid cell over each 8-day compositing period.

3.2.5 CLIMATE MODELING GRID FIRE PRODUCTS (MOD14CMH, MYD4CMH, ETC.)

The CMG fire products are gridded statistical summaries of fire pixel information intended for use in regional and global modeling. The products are currently generated at 0.5 spatial resolution for time periods of one calendar month (MOD14CMH/MYD14CMH) and eight days (MOD14C8H/MYD14C8H). Higher resolution 0.25° CMG fire products are planned for Collection 5 as well.

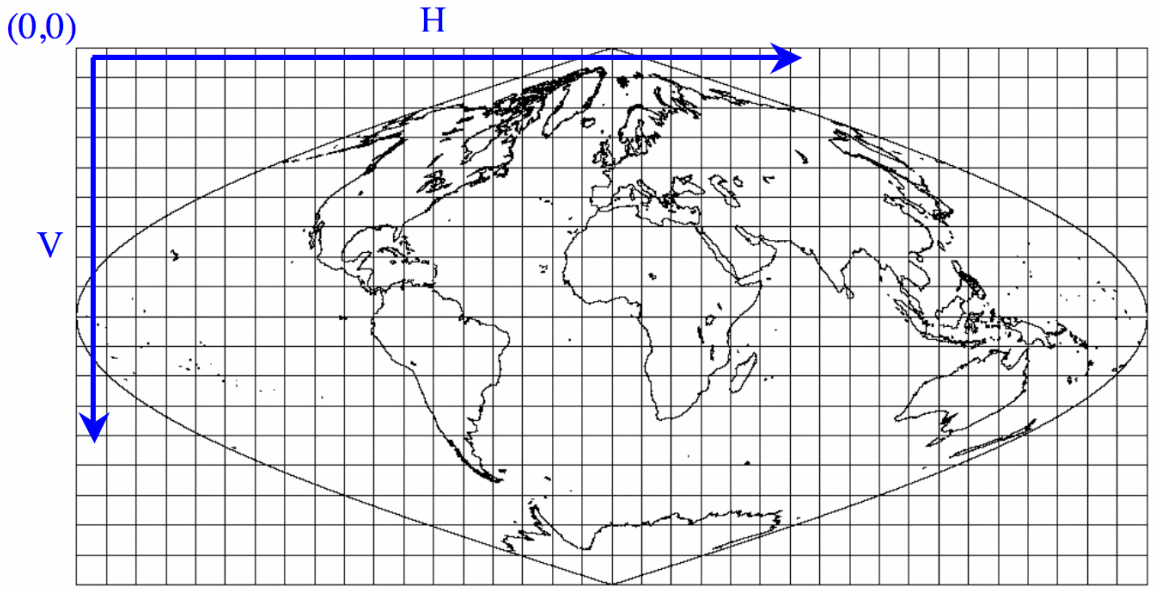

Figure 3: MODIS tiling scheme.

3.3 VALIDATION OF THE MODIS ACTIVE FIRE PRODUCTS

Stage 2 validation of the Terra MODIS fire products is nearly complete and has been based primarily on comparison with high-resolution fire maps derived from Advanced Spaceborne Thermal Emission and Reflection Radiometer (ASTER) imagery. Comparisons with small numbers of near-coincident SPOT and Bi-Spectral Infrared Detection (BIRD) scenes have been reported as well (Liew et al. 2003, Zhukov et al. 2006). Additional validation activities have been performed by the U.S. Forest Service using in situ fire observations.

3.3.1 ASTER FIRE DETECTION

Since manual production of ASTER fire masks is time consuming, and simple fixed threshold methods do not scale well (both spatially and temporally), a consistent, automated source of ASTER fire masks is desirable. For this reason, a fire detection algorithm that uses ASTER observations to provide binary "yes/no" fire masks at 30-m spatial resolution has been developed.

The general approach used in several studies (Section 3.3.2) is, for daytime scenes, to use two ASTER bands, one of which is sensitive to the black-body radiation emitted by fires (band 8), and another which is insensitive to such radiation but that provides a highly-correlated reflectance over "noramal" (non-fire) components of terrestrial scenes, which include soil, vegetation, clouds, and urban areas. Under these criteria ASTER bands 3N (0.82 μm) is the only viable candidate. Nighttime scenes, being devoid of reflected sunlight, are much less ambiguous, and active fires can be identified with thresholds applied to band 8 imagery. Details of the approach are described by Giglio (2006). A simpler, threshold-based approach appropriate for use in southern Africa is described by Morisette et al. (2005a).

3.3.2 VALIDATION RESULTS USING ASTER IMAGERY

Morisette et al. (2005a) used 18 ASTER scenes distributed throughout southern Africa covering the time period 5 August 2001 to 6 October 2001 to compare the previous Collection 3 and current Collection 4 MODIS fire products. Performance was characterized through the use of logistic regression models to establish a relationship between the binary MODIS "fire/no-fire" product and summary statistics derived from ASTER data over the coincident MODIS pixel; example results are presented in Figure 4. The authors determined probabilities of detection as a function of the total number of ASTER fires and Moran's *I*, a measure of the spatial heterogeneity of fires within the MODIS pixel. With this approach it was established that the algorithm changes have a positive effect on the fire-product accuracy.

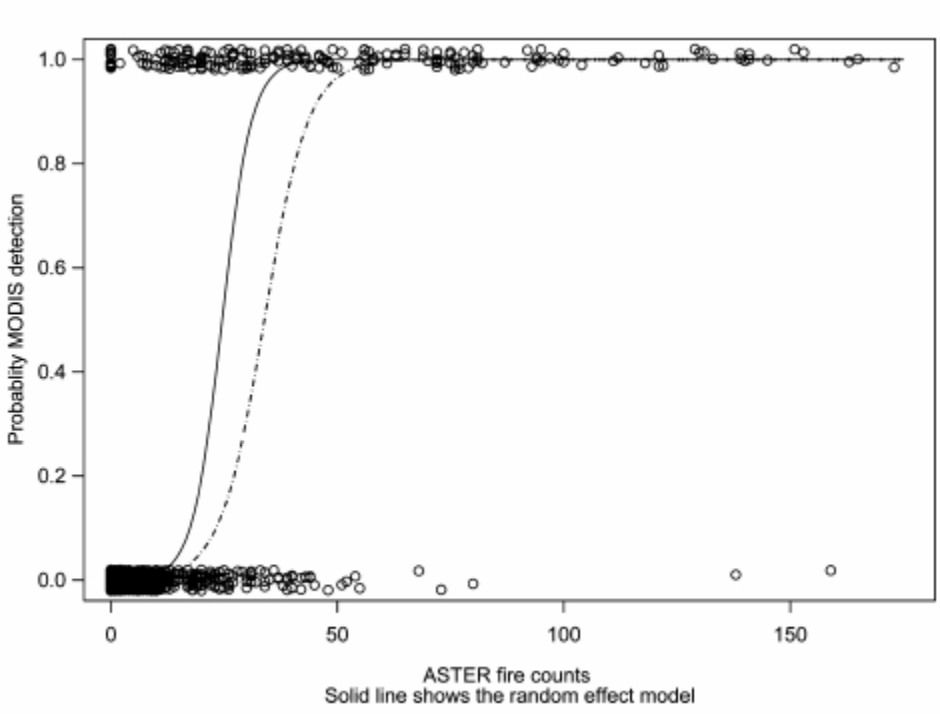

Figure 4: Estimated detection probabilities as a function of the number of ASTER fire pixels within the MODIS pixel, using the Collection 4 MODIS algorithm. Source: Morisette et al. (2005a).

Subsequent work by Morisette et al. (2005b) used ASTER fire masks to evaluate the performance of the MODIS fire detection algorithm and a regional MODIS fire detection algorithm developed by the Brazilian Instituto Nacional de Pesquisas Espaciais (INPE) in the Amazon. The authors found that, for both algorithms, the likelihood of MODIS fire detection was a function of both the number of ASTER fire pixels within the MODIS pixel, as well as the contiguity of the ASTER fire pixels. Both algorithms had similar omission errors, and each had a fairly high likelihood of detecting relatively small fires, as observed in the ASTER data. However, the commission error for the INPE algorithm was approximately 3 times larger than that of the standard MODIS algorithm.

Most recently, Csiszar et al. (2006) reported that in Siberia the size of a single ASTER fire cluster within the MODIS footprint that has a 50% probability of being detected is ~60 ASTER pixels, compared to ~45 ASTER pixels in the Amazon. This is in contrast to previous

radiative transfer simulations suggesting similar detection probabilities in the two regions. The authors attribute this discrepancy to the frequent obscuration of large Siberian fires by heavy smoke (Figure 5). Csiszar et al. go on to derive pixel-based and cluster-based fire detection rates, and show that the probability of flagging as "fire" a MODIS pixel which contains a given number of 30-m ASTER fire pixels is typically 3-5 times lower than detecting a contiguous cluster with the same number of ASTER fire pixels.

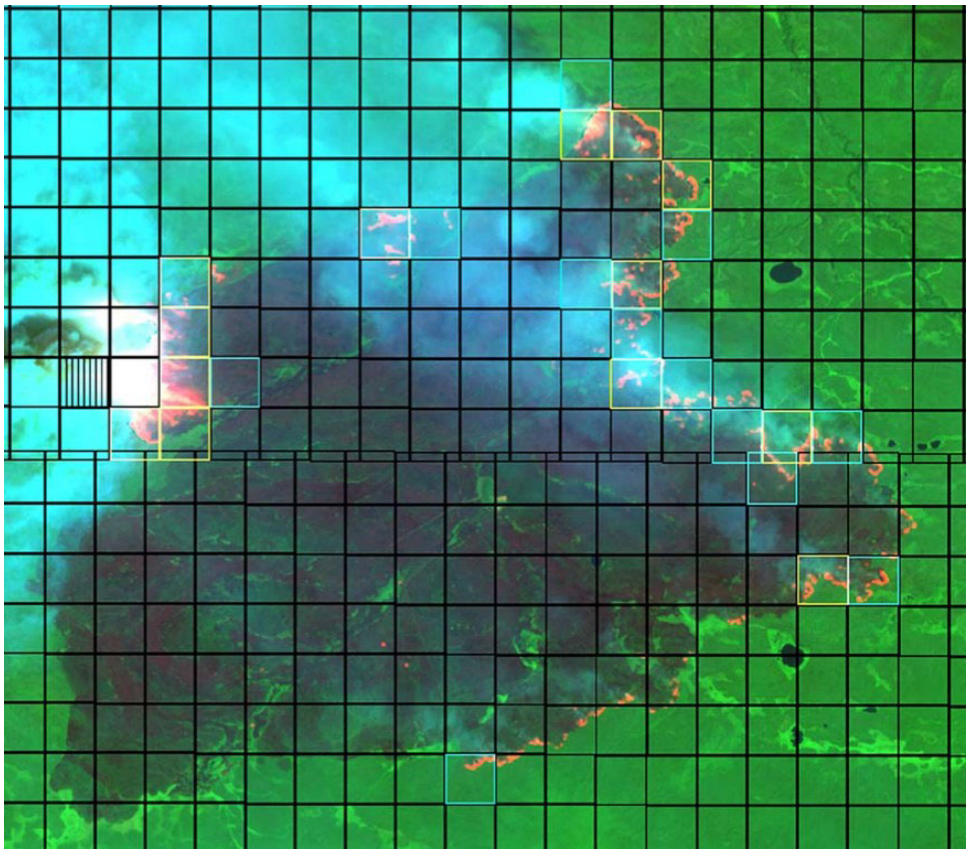

Figure 5: MODIS 1-km grids over an ASTER 8-3-1 red-green-blue image of a large fire complex on July 23, 2002. The center of the complex is approximately 63° N, 126° E. Yellow and blue MODIS cells correspond to "high" and "nominal" MODIS fire detection confidence, respectively. The pixel with vertical hatching was flagged as cloud. Source: Csiszar et al. (2006).

4.0 BURNED AREA PRODUCT THEORETICAL DESCRIPTION

4.1 THE MCD45 PRODUCT

The MODIS algorithm defined to map burned areas has been developed, demonstrated in southern Africa, Australia, Siberia and South America (Roy et al. 2002, Roy 2003), and integrated, starting with Collection 5, in the MODIS processing chain. This section overviews the main characteristics of the algorithm that has being implemented in the MODIS processing chain to map global fire-affected areas. The algorithm uses a bi-directional reflectance model-based change detection approach to map the 500 m location and approximate day of burning. It detects the approximate date of burning by locating the occurrence of rapid changes in daily MODIS Terra and Aqua reflectance time series. The algorithm maps the spatial extent of recent fires and not of fires that occurred in previous seasons or years. The burned area product is identified as MCD45A1.

4.2 INPUTS

The MODIS burned area product is generated from time series of daily 500 m MODIS land surface reflectance data. Measurements in the seven MODIS land surface reflectance bands are corrected for atmospheric effects, including aerosols (Vermote et al. 2002). These data are processed into daily geolocated files (Wolfe et al. 1998) and all high view zenith (>65°), high solar zenith (>65°), bad quality, high aerosol, snow, cloudy, and non-land, MODIS observations labelled in land surface reflectance product are rejected. These data provide good quality observations of the land surface, although shadow contaminated observations and a minority of cloud, snow, and water observations may remain. This gives a maximum of one observation per geolocated pixel per day.

4.3 MODIS BURNED AREA DISCRIMINATION ISSUES

4.3.1 WAVELENGTH SELECTION

MODIS bands that are sensitive and insensitive to biomass burning are used to detect changes due to fire and to differentiate them from other types of change respectively. The near-infrared and longer wavelength 500 m MODIS reflectance bands are used because they are generally insensitive to smoke aerosols emitted from vegetation fires (Kaufman and Remer 1994, Miura et al. 1998). An analysis of the ability of the MODIS land surface reflectance bands to discriminate between recently burned and unburned vegetation (Roy et al. 2002, 2005a) has shown that MODIS bands 5 [1230-1250 nm] and 2 [841-876 nm] pro-vide the highest burned-unburned discrimination and MODIS band 7 [2105-2155 nm] provides little discrimination. Bands 5, 2 and 6 [1628-1652 nm] reflectance decreases immediately, and for many days, after burning, and band 7 reflectance changes relatively less (with both positive or negative changes observed).

Some surface changes not associated with biomass burning may exhibit similar spectral changes as those caused by fire. Depending on the algorithm and wavelengths used this may cause false detections.

Examination of Figure 6 indicates that decreases in near-infrared and short wave infrared reflectance (MODIS bands 2 and 5) similar to those caused by burning may also occur with snow melt, vegetation removal exposing less reflective soil (e.g., due to harvesting or pests),

flooding, and vegetation senes-cence. The Australian herbaceous plant spectra (green) show a typical reduction in the near-infrared (bands 2 and 5) and increase in red (band 1) reflectance as the vegetation senesces from lush green vegetation to dried material with 100% cover. The Zambian grass spectra (orange) show an opposite change and are included to illustrate the complexity of potential sources of spectral confusion. In the Zambia case, senescence from green, waterlogged grass (dashed orange) to dry grass on an exposed bright soil background (solid orange) increases the near-infrared and the other MODIS band reflectance. The Zambian example illustrates that increasing plant water content may reduce MODIS band 5, 6 and 7 reflec-tance but have less impact on band 2 reflectance (Zarco-Tejada et al. 2003). Shadows, cast by clouds and surface relief, are not illustrated, but generally reduce reflectance in all reflective bands and so exhibit similar spectral changes as those caused by fire (Roy et al. 2002).

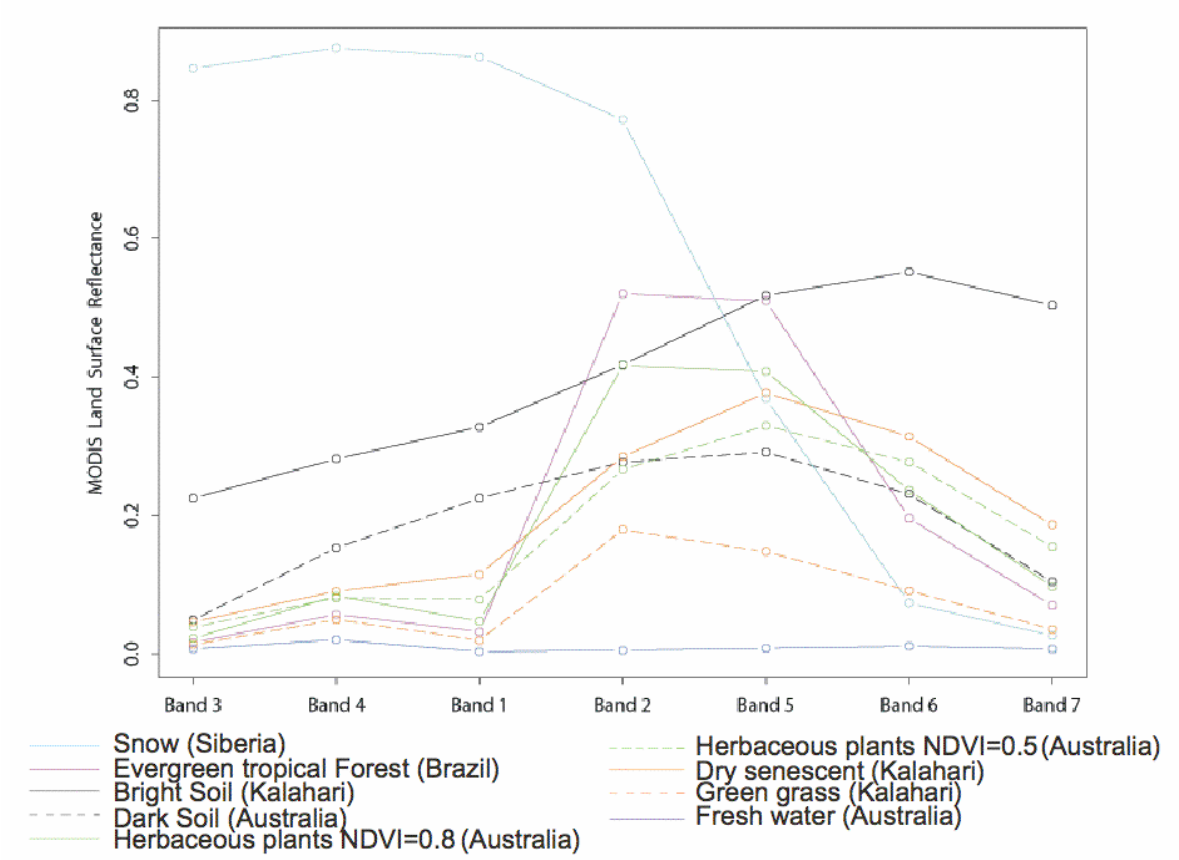

Figure 6: Illustrative MODIS reflective band spectra. Mean reflectance of 25 cloud-free, near-nadir 500 m MODIS pixels for a number of different surface types.

4.3.2 Surface Bi-directional Reflectance Effects

Wide field of view sensors, such as MODIS, AVHRR, and Spot Vegetation, sense the same point on the surface with widely varying viewing and solar angles through time. This is illustrated in Figure 7 which shows a polar plot of these angles for MODIS Terra and Aqua observations at a single pixel in Australia.

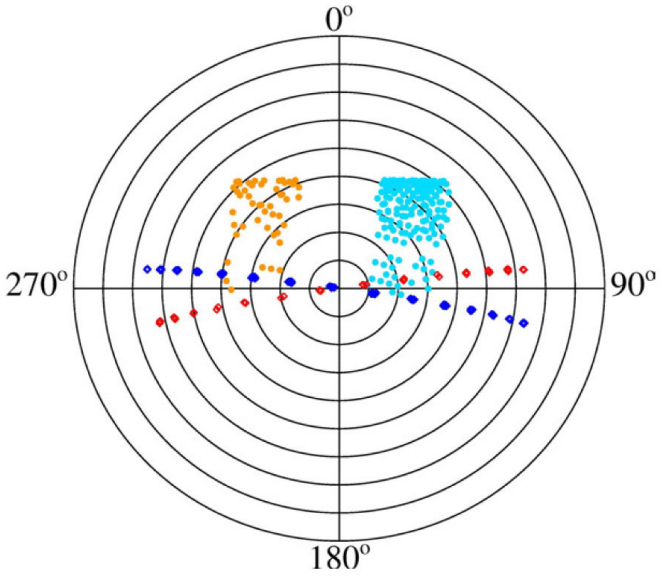

Figure 7: Polar plot showing the MODIS viewing geometry (Terra blue, Aqua red) and solar geometry (Terra cyan, Aqua orange) of 220 days of observations at a point in Australia. Radial lines show zenith increasing froom 0° at the plot center to 90° at the plot edge. Straight lines show azimuth.

The reflectance of the surface, detected by any remote sensor, varies as a function of the sun-surface-sensor angles and is described by the Bi-directional Reflectance Distribution Function (BRDF) (units of sr^{-1}) (Kimes 1983, Pinty and Verstraete 1992). Bi-directional reflectance variations complicate the identification of surface change. Recent work, based on examination of satellite data (Roy et al. 2002, Stroppiana et al. 2002, Roy et al. 2005a) and ground-based radiometric measurements (Trigg et al. 2005) have demonstrated that, BRDF effects reduce the separability between burned and unburned surfaces both in individual reflectance bands and in spectral band indices. This issue is evident in Figure 8 where the reflectance decrease due to a fire is less than the variation in pre-fire reflectance caused by BRDF effects.

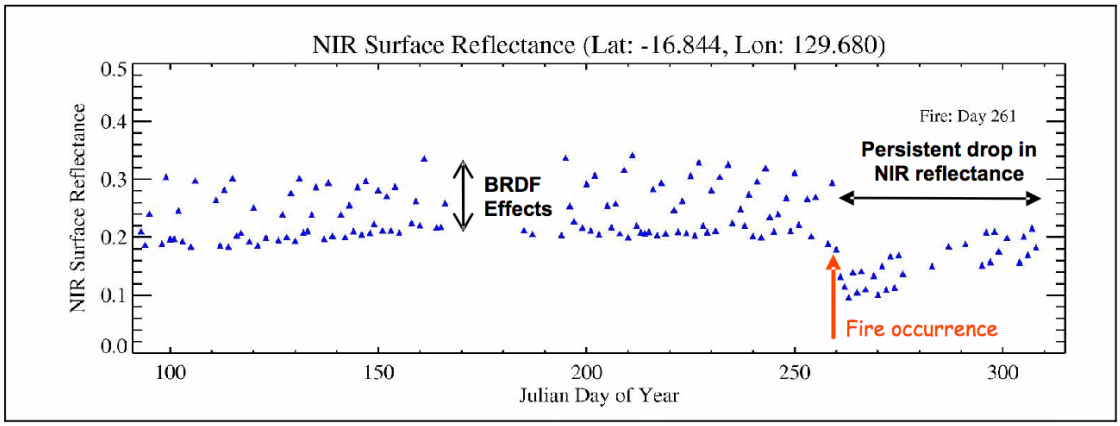

Figure 8: Time series of near infrared reflectance of a single MODIS pixel (for the angles illustrated in Fig. 7)

The majority of algorithms developed to map fire-affected areas use spectral indices. Spectral indices have attractive properties, such as reducing certain shadow, illumination and topographic induced variations (Holben and Justice 1981), but can still have significant directional effects (Gao et al. 2002, Trigg et al., 2005). Failure to account for these effects implies a commensurate reduction in change detection capabilities (Roy et al 2002). Regardless of directional effects, simple modeling work has demonstrated that ratio spectral indices may be sensitive in a non-linear manner to the size and combustion complete-ness of the fire and so may provide variable detection capabilities when used to map fire-affected areas (Roy and Landmann, 2005). This is illustrated in Figure 9.

Composited satellite data are frequently used to reduce the impact of atmospheric contamination and di-rectional effects (Holben 1986). Directional reflectance effects remain in n-day composited data (both re-flectance and spectral indices). However, restricting observations to close-to-nadir to minimize their im-pact reduces the effective temporal sampling frequency and discards the potentially useful information found in off-nadir observations (Cihlar et al. 1994).

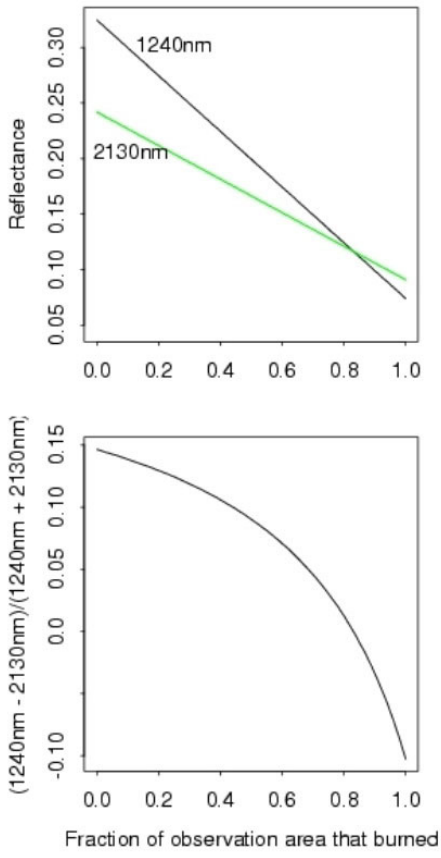

Figure 9: Linear mixture modeling results for a hypothetical observation sensed over a fire-affected area with com-bustion completeness = 0.9 plotted as a function of the fraction of the observation area that burned. Top: Reflec-tance modeled at 1240 nm and 2130 nm with spectral end members defined from field radiometric measurements of photosynthetic vegetation and black ash, Bottom: corresponding spectral index values (Roy and Landmann, 2005).

4.4 THE GLOBAL MODIS ALGORITHM FOR BURNED AREA MAPPING

The bi-directional reflectance model-based change detection algorithm is a generic change detection method that is applied independently to geolocated pixels over a long time series (weeks to months) of reflectance observations (Roy et al. 2002, 2005a). Reflectances sensed within a temporal window of a fixed number of days are used to predict the reflectance on a subsequent day. A statistical measure is used to determine if the difference between the predicted and observed reflectance is a significant change of in-terest. Rather than attempting to minimize the directional information present in wide field-of-view satellite data by compositing, or by the use of spectral indices, these information are used to model the directional dependence of reflectance. This provides a semi-physically based method to predict change in reflectance from the previous state.

4.4.1 The bi-directional reflectance model-based expectation approach

Methods have been developed to model the BRDF with a limited number of parameters and then to esti-mate the model parameters from a finite set of remotely sensed observations (Lucht 2004). The semi-empirical RossThick-LiSparse reciprocal BRDF model is used for the MODIS global fire-affected area product as it performs robustly in the global MODIS BRDF/albedo product (Schaaf et al. 2002). Like other linear kernel-driven models it allows analytical model inversion with an estimate of uncertainty in the model parameters and linear combinations thereof (Lucht and Roujean 2000, Lucht and Lewis 2000). At each geolocated pixel the three parameter RossThick-LiSparse reciprocal BRDF model is inverted against m ~ 7 reflectance observations sensed in a temporal window of n (~ 16) days duration. The BRDF model parameters are used to compute predicted reflectance and uncertainties for the viewing and illumi-nation angles of a subsequent observation. A Z-score is used as a normalized measure related to the prob-ability of the new observation belonging to the same set as that used in the BRDF model inversion:

$$Z_\lambda = \frac{\rho_{new}(\lambda,\Omega,\Omega') - \rho(\lambda,\Omega,\Omega')}{\varepsilon} \qquad (1)$$

$$\varepsilon = \sqrt{\sigma_\lambda^2 + e^2 \frac{1}{w}}$$

where

Z_λ is the Z-score value,

$\rho_{new}(\lambda,\Omega,\Omega')$ is the new reflectance observation,

$\rho(\lambda,\Omega,\Omega')$ is the model predicted reflectance at wavelength λ computed by analytical inversion of the BRDF model against previous reflectance observations,

□ and □' are the viewing and illumination vectors respectively of the new reflectance observation

σ_λ is a fixed pre-assigned estimate of the noise in $\rho_{new}(\lambda,\Omega,\Omega')$ defined by Vermote et al. (2002)

e is the root mean squared of the residuals of the BRDF inversion (used as an estimate of noise in the observations and the lack of ability of the model to fit the measurements)
w is the 'weight of determination' of $\rho_{new}(\lambda,\Omega,\Omega')$ (Lucht and Lewis 2000).

Z_λ is adaptive to the viewing and illumination angles of the new observation, as well as the angular distribution, amount of noise, and number of the observations used in the BRDF inversion. The Z-score is computed for MODIS band 2 and 5 as these bands are both sensitive to burning and decrease post-fire. A new observation is considered as a bunt candidate if :

$$(Z_{band\,2} < -Z_{thresh}) \text{ OR } (Z_{band\,5} < -Z_{thresh}) \quad (2)$$

where

Z_{band} is the Z-score defined (1)
Z_{thresh} is a fixed wavelength independent threshold.

and if:

$$\rho(\lambda_{band\,5},\Omega,\Omega') - \rho(\lambda_{band\,7},\Omega,\Omega') > \rho_{new}(\lambda_{band\,5},\Omega,\Omega') - \rho_{new}(\lambda_{band\,7},\Omega,\Omega') \quad (3)$$

AND

$$\rho(\lambda_{band\,2},\Omega,\Omega') - \rho(\lambda_{band\,7},\Omega,\Omega') > \rho_{new}(\lambda_{band\,2},\Omega,\Omega') - \rho_{new}(\lambda_{band\,7},\Omega,\Omega')$$

where $\rho_{new}(\lambda,\Omega,\Omega')$ is the new reflectance observation and $\rho(\lambda,\Omega,\Omega')$ is the model predicted reflectance computed by analytical inversion of the BRDF model against $m \geq 7$ previous reflectance observations. The justification for Eq. (3) is that burning causes a reduction in band 2 and 5 reflectance but less change in band 7 reflectance, whereas persistent cloud, shadow, or soil moisture changes would have a similar effect in both bands. Band 2 helps to remove changes associated with increasing plant water content which is negatively related to band 5 and 7 reflectance but not band 2 reflectance (Zarco-Tejada et al. 2003). In this work $Z_{thresh} = 3.0$ to detect only those reflectance changes that fall outside of the expected reflectance variation modeled from previous values (the probability that Z < -3.0 is ~0.0013). Some other spectral constraints are implemented but there is insufficient space for their description here.

4.4.2 Temporal implementation

The computation (1-3) is repeated independently for each geolocated pixel, moving through the reflectance time series in daily steps to detect change. A temporal constraint is used to differentiate between temporary changes, such as shadows, undetected residual clouds, soil moisture changes and data artifacts, that pass (1) – (3) from fire-affected areas that have persistently lower post-fire reflectance.

Gaps in the reflectance time series, for example due to cloud cover or bad quality input data, reduce the temporal frequency of Z-score calculations as they reduce the number of observations available for prediction and the number of windows that have sufficient observations for BRDF inversion. To reduce the impact of gaps, the duration of the BRDF inversion window is allowed to increase and the Z-score is computed not just for the subsequent day but for several subsequent days. This is illustrated in Figure 10. The duration of the BRDF

inversion window is allowed to increase, from a minimum of n = 16 days up to a maximum of (n + n_{extra}) days, until there are at least 7 observations. When there are fewer than 7 observations no inversion is performed. In this way, more BRDF inversions may be performed in the presence of missing data, providing more opportunities for detecting burning events. At each window containing 7 or more observations the BRDF parameters are used to compute Z-scores for the non-missing observations sensed on the following S_{search} days. If within the following S_{search} days a burn candidate is found, i.e. criteria (1)-(3) are met, then the Z-scores continue to be computed for S_{test} days after the first burn candidate.

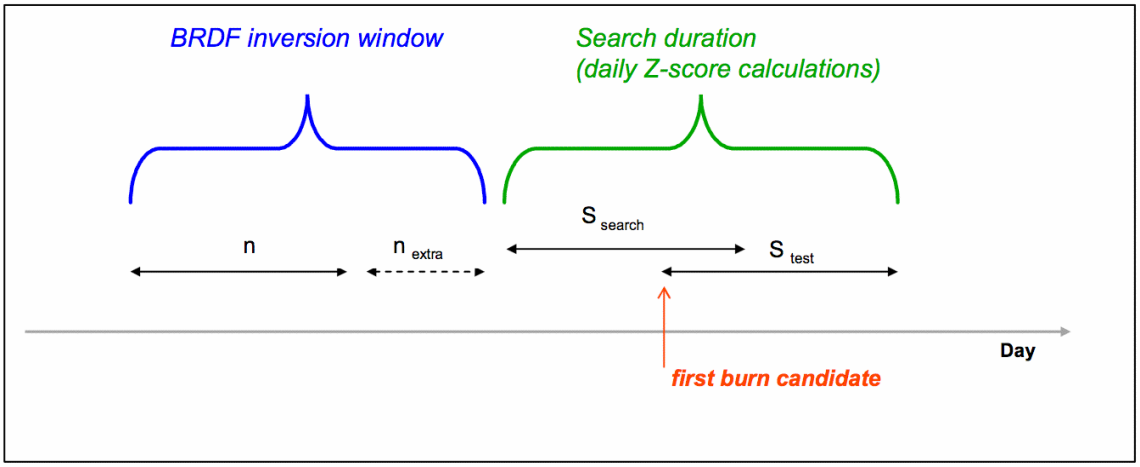

Figure 10: Conceptual scheme of the detection approach. To reduce the number of gaps, if fewer than 7 observation are available in the n days moving window, the window is expanded in an adaptive way, including up to $n+n_{extra}$ days. The prediction is computed for the following S_{search} days; if a burnt candidate is found, the persistence of the drop of the signal is tested on the subsequent S_{test} days.

For each inversion window, the day that the first burn candidate was detected (Day_{first}), the maximum of its band 2 and 5 Z-scores (Z_{first}), and the total number of observations over the subsequent S_{test} days that were considered (*Nused*) and detected as burned (N_{pass}), are derived. Different Day_{first} candidates may be detected because of sensitivity of the adaptive window duration and multi-date prediction to gaps in the time series. In addition, the same geolocated pixel may burn on separate dates. The results from the different inversion windows are ranked with respect to N_{pass} and then *Nused*, to provide results in order of the most evidence of persistent burning. If there are results with equal N_{pass} and *Nused* values then the one with the greatest $|Z_{first}|$ is ranked as more persistent. Searching both forwards and backwards in time allows burn candidates to be detected in the S_{search} days preceding or following periods of persistently missing data. This also allows burn candidates to be detected in the first and last S_{search} days of the time series. Results for the forward and backward directions are derived independently. When searching backwards in time, an increase in reflectance in the appropriate MODIS bands is searched for rather than a reflectance decrease. Illustrative results of this approach are shown in Figure 11.

4.4.3. Iterative procedure for identification of burned candidates

The global algorithm attempts to reduce errors of commission by only selecting fire-affected pixels where there are burn candidates that provide persistent evidence of fire occurrence. As the measured persistence varies depending on gaps in the reflectance time series and the timing of the fire relative to non-missing data, an iterative rather than simple thresholding approach is used. Burn candidates found in both the forward and backward directions are considered.

First, fire-affected pixels are selected as occurring on Day_{first} if:

$$N_{pass} \geq 3 \text{ AND } (N_{pass} / Nused) \geq 0.5 \text{ AND } N_{inv} \geq 3 \quad (4)$$

In this way only candidates are selected – regardless of the direction of the detection – where at least 3 and 50% of the observations considered over the subsequent S_{test} days are detected as burned, and where at least 3 inversions (N_{inv}) are used for the consistency test. If several burn candidates are found at a given pixel then they are considered in order of decreasing evidence of persistent burning and the first one that passes (8) is selected. If forward and backward search results have equal persistence then the forward direction results are given precedence.

In cloudy regions, even confidently detected burn candidates might have insufficient data for 3 inversion within the timeframe of the consistency test. As a consequence, if – and only if – backwards and forwards predict the same change, fire affected pixels are selected, regardless of N_{inv} using the less restrictive test:

$$N_{pass} \geq 3 \text{ AND } (N_{pass} / Nused) \geq 0.5 \quad (5)$$

Second, rather than discard burn candidates that are likely to be burned but do not pass (4) and (5) because of insufficient observations, for example, in Figure 6 several burned pixels have N_{pass} less than 3 (shown as purple), they are considered using less restrictive criteria than (4) or (5), and an iterative search method. This method is based on the principle that there is increasing expectation of a burn occurring in pixels neighboring confidently detected burns (Roy et al. 2002a, Graetz et al. 2003). In this search procedure, the burn candidates selected by (4) and (5) are considered seed pixels.

In the first set of iterations, non-seed pixels where burn candidates were detected that did not pass (4) or (5) are accepted as burned if they have two or more adjacent seed neighbors and if:

$$|Day_{first} - \overline{Day_{first\_seed}}| < N_{gap} \text{ AND } N_{pass} \geq 2 \text{ AND } (N_{pass} / Nused) \geq 0.25 \quad (6)$$

where Day_{first}, N_{pass}, and $Nused$ are the values for the burn candidate that did not pass (4) or (5) and $\overline{Day_{first\_seed}}$ is the mean Day_{first} value of the two to eight adjacent seed pixels. The N_{gap} constraint ensures that only burn candidates that occur temporally as well as spatially close to the neighboring seed pixels are considered. This procedure is repeated in an exhaustive iterative manner with the pixels that passed (6) being considered as seeds for the next iteration until no more burn candidates that pass (6) can be included. As with (4), if several burn candidates are

found at a given pixel then they are considered in order of decreasing evidence of persistent burning until (6) is met. Again, if forward and backward search results have equal persistence then the forward direction results are given precedence.

In the second part of the procedure, the residual burn candidates, not selected in the previous steps, are considered if at lest three neigbours have been selected. The average day of burning of the neighbours is computed, and the pixel is accepted if the backwards of forwards day, closest to the average day, is less than N_{gap} days apart. No other thresholds are used, and this step is not iterated.

Pixels where throughout the time series there were insufficient observations to invert the BRDF model are labeled with a unique code (10000) so that they are not subsequently mistaken as being unburned.

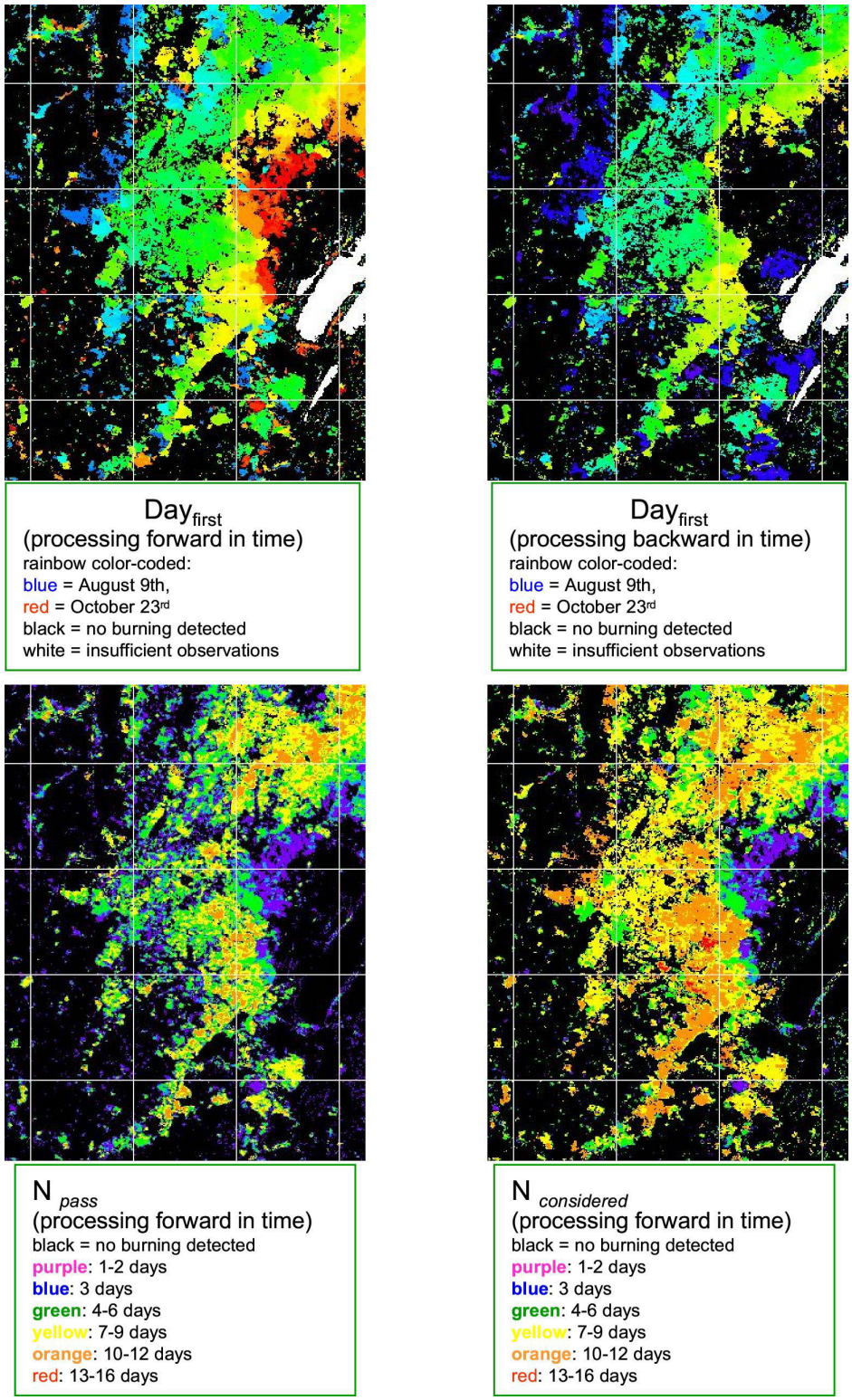

Figure 11: Example $Day_{first,}$ $N_{pass,}$ Nused results for 75 days of extensive burning, Zambia (gridline spacing 75 km).

4.5. DATA FORMAT

The product is distributed in the standard MODIS land Hierarchical Data Format, and includes the following data layers, defining for each 500m pixel:

- "Burndate"[2-byte integer]: the approximate day of burning from eight days before the beginning of the month to eight days after the end of the month.
    - 1-366 approximate day of burning
    - 900 snow
    - 9998 water bodies (Seas and Oceans)
    - 9999 water bodies (internal)
    - 10000 not enough data to perform inversion throughout the period
- "BA pixel QA"[1 byte] confidence of the detection. Values 1 (most confident) to 4 (least confident):
    - 1: most confidently detected pixels, regardless of direction (forwards, backwards or both), passing the test (4) of paragraph 4.3.
    - 2: pixels where backwards and forwards direction predict the same change, which pass the test (5)
    - 3: pixels selected in the first stage of the contextual analysis.
    - 4: pixels selected in the second stage of the contextual analysis
- "Number of Passes" [1 byte]: $N_{pass,}$ number of observations, where the temporal consistency test is passed.
    - 1 byte, unsigned
- "Number Used" [1 byte]: *Nused* number of observations used in the temporal consistency test
    - 1 byte, unsigned
- "Direction" [1 byte]: direction in which burning was detected (forward in time, backward or both)
    - 1 forwards
    - 2 backwards
    - 3 both
- "Surface Type" [1 byte]: information describing the land cover type and properties. 2 Bytes, bit-packed. From Most Significant bit:
    - The burned area detection is rejected, and the relevant bit is set to 1 if (from Least Significant to Most Significant Bit):
        - bit 0: water (NDVI < 0.1 and b7 < 0.04)
        - bit 1: low NDVI (NDVI < 0.1)

- bit 2: shallow, ephemeral, deep inland water (QA from MOD09 = 3, 4, 5 AND NDVI <0.1
- bit 3: cloud (from MOD09 internal cloud mask)
- bit 4: cloud shadow (from MOD09 internal cloud mask)
- bit 5: View and Sun zenith angle mask (Vz > 65^o threshold OR Sz > 65^o)
- bit 6: High View and Sun zenith angle (Vz > 50^o and Sz > 55^o)
- bit 7: Snow or high aerosol (from MOD09 QA) and high view / Sun zenith (Vz > 55^o AND Sz > 55^o).

- "Gap Range 1"[2 bytes]: information describing the largest number of missing/cloudy days (if any) in the time series; specifically the number of consecutive days with missing observations and the start day of this missing period.
  - 2 bytes, bit packed. From Least Significant Bit
    - bits 0-8: julian day of start of the gap
    - bit 9-13: number of missing days including start day
- "Gap Range 2"[2 bytes]: information describing the second largest number of missing/cloudy days (if any) in the time series; specifically the number of consecutive days with missing observations and the start day of this missing period.
  - 2 bytes, bit packed. From Least Significant Bit
    - bits 0-8: julian day of start of the gap
    - bit 9-13: number of missing days including start day

Acknowledgments

The authors wish to thank the contributors to the IGBP-DIS Fire Algorithm Workshop Report (Don Cahoon, Pete Dowty, Eric Kasischke, Jackie Kendall, Elaine Prins). Material from the IGBP report has been included in the first part of this document.

REFERENCES

Andreae, M.O., E.V. Browell, M. Garstang, G.L. Gregory, R.C. Harriss, G.F. Hill, D.J. Jacob, M.C. Pereira, G.W. Sachse, A.W. Setzer, P.L. Silva Dias, R.W. Talbot, A.L. Torres, S.C. Wofsy, 1988, Biomass-burning and associated haze layers over Amazonia, *Journal of Geophysical Research*, 93:1509-1527.

Andreae, M. O., 1991: Biomass burning: its history, use, and distribution and its impact on environmental quality and global climate. In: Global Biomass Burning, p. 3-21, J. S. Levine(Ed.). Cambridge, MA: The MIT Press.

Browell, E. V., G. L. Gregory and R.C. Harriss, 1988: Tropospheric ozone and aerosol distributions across the Amazon Basin. *Journal of Geophysical Research*, 93, 1431-1451.

Charlson, R. J., J. Langner, H. Rodhe, C.B. Leovy and S.G. Warren, 1991: Perturbation of the northern hemisphere radiative balance by backscattering from anthropogenic sulfate aerosols. *Tellus*, 43AB, 152-163.

Cihlar, J., Manak, D., and D'Iorio, M., 1994. Evaluation of Compositing Algorithms for AVHRR Data Land, *IEEE Transactions on Geoscience and Remote Sensing*, 32(2):427-437.

Csiszar, I., Morisette, J. T., and Giglio, L., 2006, Validation of active fire detection from moderate resolution satellite sensors: the MODIS example in Northern Eurasia. *IEEE Transactions on Geosciences and Remote Sensing*, 44, 1757-1764, doi:10.1109/TGRS.2006.875941.

Coakley, J.A., Jr. and F.P. Bretherton, 1982, Cloud cover from high-resolution scanner data: detecting and allowing for partially filled fields of view, *Journal of Geophysical Research*, 87:4917-4932.

Coakley, J. A. Jr., R. D. Cess and F. B. Yurevich, 1983: The effect of tropospheric aerosol on the earth's radiation budget: a parameterization for climate models. *Journal of Atmospheric Science*, 40, 116-138.

Coakley, J. A. Jr., R. L. Bernstein and P. A. Durkee, 1987: Effect of ship stack effluents on cloud reflectivity. *Science*, 237, 1020-1022.

Cracknell, A.P., 1993, A method for the Correction of Sea Surface Temperatures derived from satellite thermal infrared data in an area of sunglint, *International Journal of Remote Sensing*, 14:3-8.

Crutzen, P. J. and M. O. Andreae, 1990: Biomass burning in the tropics: impact on atmospheric chemistry and biogeochemical cycles. *Science*, 250, 1669-1678.

Crutzen, P.J., A. C. Delany, J. Greenburg, P. Haagensen, L. Heidt, R. Lueb, W. Pollock, W. Seilor, A. Wartburg, and P. Zimmerman, 1985: Tropospheric chemical composition measurements in Brazil during the dry season. *Journal of Atmospheric Chemistry*, 2, 233-256.

Dozier, J., 1981, A method for satellite identification of surface temperature fields of subpixel resolution, *Remote Sensing of Environment*, 11:221-229.

Fishman, J., P. Minnis and H.G. Reichle Jr., 1986, Use of satellite data to study tropospheric ozone in the tropics, *Journal of Geophysical Research*, 91: 14451-14465

Gao, F., Jin, Y., Xiaowen, L., Schaaf, C.B., Strahler, A.H., 2002, Birdirectional NDVI and atmospherically resistant BRDF inversion for vegetation canopy, *IEEE Transactions on Geoscience and Remote Sensing*, 40, 1269-1278.

Giglio, L., Csiszar, I., Morisette, J. T., Schroeder, W., Morton, D., and Justice, C. O., 2006, Active Fire Detection with the Advanced Spaceborne Thermal Emission and Reflection Radiometer, manuscript in preparation.

Giglio, L., Descloitres, J., Justice, C. O., and Kaufman, Y., 2003, An enhanced contextual fire detection algorithm for MODIS. *Remote Sensing of Environment*, 87:273-282.

Greenburg, J. P., P. R. Zimmerman, L. Heidt and W. Pollock, 1984: Hydrocarbon and carbon monoxide emissions from biomass burning in Brazil. *Journal of Geophysical Research*, 89, 1350-1354.

Hallett, J., J. G. Hudson and C.F. Rogers, 1989: Characterization of combustion aerosols for haze and cloud formation. *Aerosol Sci. and Tech.*, 10, 70-83.

Holben, B, 1986, Characteristics of maximum-value composite images from temporal AVHRR data, *International Journal of Remote Sensing*, 7, 1417-1434.

Holben, B. and Justice, C., 1981, An examination of spectral band ratioing to reduce the topographic effect in re-motely sensed data, *International Journal of Remote Sensing*, 2, 115-133.

Hudson, J.G., 1991: Observations of anthropogenic cloud nuclei. *Atmospheric Environment*, 25A, 2449-2455.

Justice, C. O., Giglio, L., Korontzi, S., Owens, J., Morisette, J., Roy, D., Descloitres, J., Alleaume, S., Petitcolin, F., and Kaufman, Y., 2002, The MODIS fire products. *Remote Sensing of Environment*, 83:244-262.

Kaufman, Y.J. and T. Nakajima, 1993: Effect of Amazon smoke on cloud microphysics and albedo-analysis from satellite imagery. *Journal of. Applied Meteorology*, 32, 729-744.

Kaufman, Y.J., A. Setzer, C. Justice, C.J. Tucker, M.C. Pereira and I. Fung, 1990a, Remote Sensing of Biomass Burning in the Tropics, In: *Fire in the Tropical Biota: Ecosystem Processes and Global challenges*, J.G. Goldammer (ed.), Springer-Verlag, Berlin, pp371-399.

Kaufman, Yoram J., Compton J. Tucker and Inez Fung, 1990b, Remote Sensing of Biomass Burning in the Tropics, *Journal of Geophysical Research*, 95(D7):9927-9939.

Kaufman, Y.J., R.S. Fraser and R.L. Mahoney, 1991: Fossil fuel and biomass burning effect on climate-heating or cooling? *Journal of Climate*, 4, 578-588.

Kaufman, Y. J., A. Setzer, D. Ward, D. Tanre, B. N. Holben, P. Menzel, M. C. Pereira and R. Rasmussen, 1992: Biomass Burning Airborne and Spaceborne Experiment in the Amazonas (BASE-A). *Journal of Geophysical Research*, 97, 14581-14599.

Kaufman, Y. J., Justice, C. O., Flynn, L. P., Kendall, J. D., Prins, E. M., Giglio, L., Ward, D. E., Menzel, W. P., and Setzer, A. W., 1998, Potential global fire monitoring from EOS-MODIS. *Journal of Geophysical Research*, 103:32215-32238.

Kaufman, Y.J. and Remer, L., 1994, Detection of forests using mid-IR reflectance: An application for aerosol stud-ies, IEEE Transactions on Geoscience and Remote Sensing, 32:672-683.

Kimes D.S., 1983, Dynamics of Directional Reflectance Factor Distributions for Vegetation Canopies, Applied Op-tics, 22:1364-1372.

Leaitch, W.R., G.A. Isaac, J.W. Strapp, C.M. Banic and H.A. Wiebe, 1992: The relationship between cloud droplet number concentrations and anthropogenic pollution: observations and climatic implications. *Journal of Geophysical Research*, 97, 2463-2474.

Levine, J. S., 1991: Global biomass burning: atmospheric, climatic, and biospheric implications. In: *Global Biomass Burning*, J. S. Levine (Ed.). Cambridge, MA: The MIT Press.

Liew, S. C., Shen, C., Low, J., Lim, A., and Kwoh, L. K., 2003, Validation of MODIS fire product over Sumatra and Borneo using High Resolution SPOT Imagery. Proc. of the 24th Asian Conference on Remote Sensing & 2003 International Symposium on Remote Sensing, Volme 1, 671-673.

Lucht, W., 2004, Viewing the Earth from multiple angles: Global change and the science of multiangular reflectance. In: *Reflection Properties of Vegetation and Soil with a BRDF Data*

base, Eds. M. von Schonermark, B. Geiger, and H.P.Roser, Wissenschaft und Technik Verlag, Berlin.

Lucht, W. and Lewis, P.E., 2000, Theoretical noise sensitivity of BRDF and albedo retrieval from the EOS-MODIS and MISR sensors with respect to angular sampling, *International Journal of Remote Sensing*, 21:81-98.

Lucht, W., and Roujean, J-L., 2000, Considerations in the Parametric Modeling of BRDF and Albedo from Mul-tiangular Satellite Sensor Observations, *Remote Sensing Reviews*, 18:343-379.

Malingreau, J.P., 1990, The contribution of remote sensing to the global monitoring of fires in tropical and subtropical ecosystems, In: Goldammer, J.G. (ed.), Fires in tropical biota, Ecol. Studies 82, Springer, Berlin, pp.337-370.

Matson, M. and J. Dozier, 1981, Identification of subresolution high temperature sources using a thermal IR sensor, Photo. Engr. and Remote Sensing, 47(9):1311-1318.

Matson, Michael and Brent Holben, 1987, Satellite detection of tropical burning in Brazil, *International Journal of Remote Sensing*, 8(3):509-516.

Matson, Michael, Stanley R. Schneider, Billie Aldridge and Barry Satchwell, 1984, Fire Detection Using the NOAA-Series Satellites, NOAA Technical Report NESDIS 7, 34pp.

McClain, E. Paul, William G. Pichel and Charles C. Walton, 1985, Comparative Performance of AVHRR-Based Multichannel Sea Surface Temperatures, *Journal of Geophysical Research*, 90(C6):11587-11601.

Miura, T., Huete, A.R., van Leeuwen, W.J.D, Didan, K., 1998, Vegetation detection through smoke filled AVIRIS images: An assessment using MODIS band passes, Journal of Geophysical Research, 103 (D24):32001-32011.

Molion, L.C.B., 1991, Amazonia: burning and global climate impacts, In: Global Biomass Burning, p. 457-462, J.S. Levine (Ed.). Cambridge, MA, The MIT Press.

Morisette, J., Giglio, L., Csiszar, I., and Justice, C. O., 2005a, Validation of the MODIS Active fire product over Southern Africa with ASTER data. *International Journal of Remote Sensing*, 26:42394264.

Morisette, J. T., Giglio, L., Csiszar, I., Setzer, A., Schroeder, W., Morton, D., and Justice, C. O., 2005b, Validation of MODIS active fire detection products derived from two algorithms. *Earth Interactions*, 9(9):1-25.

Nath, A. Narendra, M.V. Rao and K.H. Rao, 1993, Observed high temperatures in the sunglint area over the ocean. *International Journal of Remote Sensing*, 14(5):849-853.

Penner, J. E., R. E. Dickenson, C. A. O'Neill, 1992: Effects of aerosol from biomass burning on the global radiation budget. *Science*, 256, 1432-1434.

Pinty, B. and Verstraete, M., 1992, On the design and validation of bidirectional reflectance and albedo models, *Remote Sensing of Environment*, 41, 155-167.

Radke, L. F., J. H. Lyons, P. V. Hobbs, D. A. Hegg, D. V. Sandberg and D. E. Ward, 1990: Airborne monitoring and smoke characterization of prescribed fires on forest lands in western Washington and Oregon. Gen. Tech. Rep. PNW-GTR-251, Portland, OR: U.S.D.A., Forest Service, Pacific Northwest Research Station.

Rogers, C.F., J.G. Hudson, B. Zielinska, R.L. Tanner, J. Hallett and J.G. Watson, 1991: Cloud condensation nuclei from biomass burning. In: Global Biomass Burning, p. 431-438,

Roy, D., Borak, J, Devadiga, S., Wolfe, R., Zheng, M., Descloitres, J., 2002, The MODIS land product quality assessment approach, *Remote Sensing of Environment*, 83:62-76.

Roy D.P., Lewis P.E., Justice C.O., 2002a, Burned area mapping using multi-temporal moderate spatial resolution data – a bi-directional reflectance model-based expectation approach. Remote Sensing of Environment, 83:263-286.

Roy, D.P. and Landmann, T., 2005, Characterizing the surface heterogeneity of fire effects using multi-temporal reflective wavelength data, International Journal of Remote Sensing, 26:4197-4218.

Roy, D.P., Jin, Y., Lewis, P.E., Justice, C.O., 2005a, Prototyping a global algorithm for systematic fire-affected area mapping using MODIS time series data, *Remote Sensing of Environment*, 97: 137-162.

Roy, D.P., 2003, SAFARI 2000 July and September MODIS 500m Burned Area Products for Southern Africa, in SAFARI 2000 CD-ROM Series. Volume 3. J. Nickeson, et al. eds. CD-ROM. National Aeronautics and Space Administration, Goddard Space Flight Center, Greenbelt, Maryland, USA.

Schaaf, C. B., F. Gao, A. H. Strahler, W. Lucht, X. Li, T. Tsang, N. Strugnell, X. Zhang, Y. Jin, J.-P. Muller, P.E. Lewis, M. Barnsley, P. Hobson, M. Disney, G. Roberts, M. Dunderdale, R. P. d'Entremont, B. Hu, S. Liang, J. Privette, Roy, D.P, 2002, First Operational BRDF, Albedo and Nadir Reflectance Products from MODIS, *Remote Sensing of Environment*, 83:135-148.

Stith, J.L., L.F. Radke and P.V. Hobbs, 1981: Particle emissions and the production of ozone and nitrogen oxides from the burning of forest slash. *Atmospheric Environment*, 15, 73

Trigg, S., Roy, D., Flasse, S., An in situ study of the effects of surface anisotropy on the remote sensing of burned savannah, 2005, *International Journal of Remote Sensing*, in press.

Twomey, S.A.,1977: The influence of pollution on the short wave albedo of clouds. J. Atmos.Sci., 34, 1149-1152.

Twomey, S. A., M. Piepgrass and T. L. Wolfe, 1984: An assessment of the impact of pollution on the global cloud albedo. *Tellus*, 36b, 356-366.

Twomey, S.A., 1991: Aerosols, clouds, and radiation. *Atmospheric Environment*, 25A, 2435-2442.

Vermote E. F., El Saleous N.Z., Justice C.O., 2002, Operational atmospheric correction of the MODIS data in the visible to middle infrared: first results, *Remote Sensing of Environment*, 83, 97-111.

Wolfe, R.E, Roy, D.P, Vermote, E.F., (1998), The MODIS land data storage, gridding and compositing methodology: L2 Grid, *IEEE Transactions on Geoscience and Remote Sensing*, 36:1324-1338.

Ward, D.E., R. Susott, J. Kauffman, R. Babbitt, B. N. Holben, Y.J. Kaufman, A. Setzer, R. Rasmussen, D. Cumming and B. Dias, 1992: Emissions and burning characteristics of biomass fires for cerrado and tropical forest regions of Brazil - BASE-B experiment', *J. Geophys. Res*., 97, 14601-14619.

Zarco-Tejada, P.J., Rueda, C.A., and Ustin, S.L., 2003, Water content estimation in vegetation with MODIS reflec-tance data and model inversion methods, *Remote Sensing of Environment*, 85(1), 109-124.

Zhukov, B., Lorenz, E., Oertel, D., Wooster, M., and Roberts, G., 2006, Spaceborne detection and characterization of fires during the bi-spectral infrared detection (BIRD) experimental small satellite mission (2001-2004), *Remote Sensing of Environment*, 100, 29-51.